2688 *Chem. Mater.* **2009,** *21,* 2688–2695
DOI:10.1021/cm9000569

CHEMISTRY OF MATERIALS
Article

X-ray Photoelectron Spectroscopy and in Situ X-ray Absorption Spectroscopy Studies on Reversible Insertion/Desertion of Dicyanamide Anions into/from Manganese Oxide in Ionic Liquid

Jeng-Kuei Chang,*[,†] Ming-Tsung Lee,[†] Wen-Ta Tsai,[†] Ming-Jay Deng,[‡] and I-Wen Sun[‡]

[†]*Department of Materials Science and Engineering and* [‡]*Department of Chemistry, National Cheng Kung University, 1 University Road, Tainan 701, Taiwan*

Received January 8, 2009. Revised Manuscript Received April 22, 2009

Pseudocapacitive characteristics of manganese (Mn) oxide were recognized in aprotic ionic liquid (IL), namely, butylmethylpyrrolidinium−dicyanamide (BMP−DCA), within a potential window of 3 V. The electrochemical energy storage mechanism was examined using X-ray photoelectron spectroscopy and in situ X-ray absorption spectroscopy. It was confirmed that the DCA^- anions, instead of the bigger BMP^+ cations, were the working species that compensate the Mn valent state variation upon charging and discharging in the IL electrolyte. During oxidation of the Mn oxide electrode, to keep the charges balanced, the quasi-linear DCA^- anions were inserted into the tunnels between the MnO_6 octahedral units, expanding the structural framework. Importantly, a highly reversible process was observed during the subsequent reduction step. XPS depth profiling analyses showed that the electrochemical reaction thickness was approximately 50 nm.

1. Introduction

Ionic liquids (ILs)—salts with melting points below 100 °C—have received increasing academic and industrial interest over the past decade. Their physical and chemical properties can be modified by selecting the appropriate cation/anion combination.[1] Because IL properties can be tuned over a wide range, ILs are considered "task specific" liquids.[2] Characterized by high ionic conductivity, large electrochemical windows, excellent thermal stability, nonvolatility, nonflammability, and nontoxicity, ILs have attracted enormous interest for applications in synthesis, catalysis, analysis, separation, photoluminescence, and electrochemistry.[3−7] Recently, ILs have also been used as electrolytes in energy storage devices.[8−10]

Manganese (Mn) oxides in various oxidation states and microstructures have been widely studied due to their availability, cost-effectiveness, and environmental benign characteristics for potential applications in several fields, for example, ion and molecular sieving,[11,12] catalysis,[13,14] electrochrome,[15] ion exchange,[16,17] magnetic applications,[18] and cathode material for primary alkaline cells[19,20] or rechargeable lithium batteries.[21,22] The structural frameworks of MnO_2 are composed of MnO_6 octahedral subunits, which can be linked to neighboring octahedral units by sharing corners or edges. The piling up of MnO_6 units enables the building of one-, two-, or three-dimensional tunnels, forming the various polymorphs of MnO_2 (such as α, β, γ, and δ types). In natural minerals, these tunnels are typically filled with foreign alkaline and alkaline-earth cations or water molecules; correspondingly, Mn^{4+} varies to Mn^{3+} to keep the charge neutrality.

In recent years, because of environment issues and the depletion of fossil fuels, the development of alternative energy conversion/storage systems that can meet present day power demands has accelerated. Supercapacitors are

*Corresponding author. Telephone number: +886-6-2757575 ext. 62942. Fax number: +886-6-2754395. E-mail: catalyst@mail.mse.ncku.edu.tw.

(1) Wasserchied, P.; Welton, T. Ionic Liquids in Synthesis; Wiley-VCH: Weinheim, 2003.
(2) Visser, A. E.; Swatlowski, R. P.; Reichert, W. M.; Mayton, R.; Sheff, S.; Wierzbicki, A.; Davis, J. H.; Rogers, R. D. *Chem. Commun.* **2001**, 135.
(3) Huang, J. F.; Luo, H.; Liang, C.; Sun, I. W.; Baker, G. A.; Dai, S. *J. Am. Chem. Soc.* **2005**, *127*, 12784.
(4) Enders, F.; Abedin, S. Z. E. *Phys. Chem. Chem. Phys.* **2006**, *8*, 2101.
(5) Earle, M. J.; Esperanca, J.; Gilea, M. A.; Lopes, J. N. C.; Rebelo, L. P. N.; Magee, J. W.; Seddon, K. R.; Widegren, J. A. *Nature* **2006**, *439*, 831.
(6) Wasserchied, P. *Nature* **2006**, *439*, 797.
(7) Ohno, H. Electrochemical Aspects of Ionic Liquids; John Wiley & Sons: Hoboken, 2008.
(8) Balducci, A.; Bardi, U.; Caporali, S.; Mastragostino, M.; Soavi, F. *Electrochem. Commun.* **2004**, *6*, 566.
(9) Frackowiak, E.; Lota, G.; Pernak, J. *Appl. Phys. Lett.* **2005**, *86*, 164104.
(10) Lazzari, M.; Mastragostino, M.; Soavi, F. *Electrochem. Commun.* **2007**, *9*, 1567.
(11) Segal, S. R.; Park, S. H.; Suib, S. L. *Chem. Mater.* **1997**, *9*, 98.
(12) Shen, X. F.; Ding, Y. S.; Liu, L.; Cai, J.; Laubernds, K.; Zerger, R. P.; Vasiliev, A.; Aindow, M.; Suib, S. L. *Adv. Mater.* **2005**, *17*, 805.
(13) Johns, M.; Landon, P.; Alderson, T.; Hutchings, G. J. *Chem. Commun.* **2001**, 2454.
(14) Einaga, H.; Futamura, S. *J. Catal.* **2004**, *227*, 304.
(15) Chigane, M.; Ishikawa, M. *J. Electrochem. Soc.* **2000**, *147*, 2246.
(16) Giraldo, O.; Brock, S. L.; Willis, W. S.; Marquez, M.; Suib, S. L.; Ching, S. *J. Am. Chem. Soc.* **2000**, *122*, 9330.
(17) Brock, S. L.; Sanabria, M.; Nair, J.; Suib, S. L.; Ressler, T. *J. Phys. Chem. B* **2001**, *105*, 5404.
(18) Seo, W. S.; Jo, H. H.; Lee, K.; Kim, B; Oh, S. J.; Park, J. T. *Angew. Chem., Int. Ed.* **2004**, *43*, 1115.
(19) Donne, S. W.; Lawrance, G. A.; Swinkels, D. A. J. *J. Electrochem. Soc.* **1997**, *144*, 2961.
(20) Kannan, A. M.; Bhavaraju, S.; Prado, F.; Manivel Raja, M.; Manthiram, A. *J. Electrochem. Soc.* **2002**, *149*, A483.
(21) Franger, S.; Bach, S.; Farcy, J.; Pereira-Ramos, J. P.; Baffier, N. *J. Power Sources* **2002**, *109*, 262.
(22) Abou-El-Sherbini, K. S.; Askar, M. H. *J. Solid State Electrochem.* **2003**, *7*, 435.

 Published on Web 06/04/2009

energy-storage devices that have a greater power density and a longer cycle life than those of batteries and a higher energy density than that of conventional capacitors.[23] Accordingly, they have been considered for use in hybrid electric vehicles, consumer electronics, medical electronics, and military missile systems. Mn oxide, which can undergo reversible, continuous, and faradic Mn^{4+}/Mn^{3+} redox transitions in aqueous electrolytes and thus contributes to pseudocapacitance,[24−26] has been reported to be a promising electrode material for supercapacitors. A charge storage mechanism based on a double-injection process, involving the reversible uptake of small cations (for example, H^+, Li^+, Na^+, or K^+) and electrons, has been proposed.[27−30] However, due to the intrinsic characteristics of water decomposition, aqueous electrolytes have narrow potential windows (typically ~1 V), which limit the capacitor cell voltage. Since both energy density and power density of a supercapacitor depend on the square of the cell voltage, finding an electrolyte with a large potential window of stability is critical. Although some organic solvents are stable over a relatively wide potential range, they pose serious health and safety hazards as they are volatile, flammable, and sometimes toxic. In view of these obstacles, IL seems to be a promising electrolyte for high performance supercapacitors even though Rochefort et al.[31] suggested that a redox transition of metal can only be achieved in protic (i.e., with protons) IL. In the absence of H^+, Li^+, Na^+, or K^+ cations in the electrolyte, are there other species that can be incorporated into the Mn oxide structure and, if so, what is the reaction mechanism? These issues, which have never been understood, should be clarified.

Starting from 2005, X-ray photoelectron spectroscopy (XPS) has proven to be a powerful tool in investigating the elemental composition and the chemical state of ILs[32−35] because of the surface sensitivity of the core level electron binding energies to the local chemical environment. Recently, XPS has also been used for identifying surface contamination or surface enrichment of dissolved species,[36−38] for quantifying the solubility of some species,[39] and for determining the chain orientation on the topmost interfacial surface of ILs.[40,41] X-ray absorption spectroscopy (XAS), normally divided into two regions—the X-ray absorption near edge structure (XANES) and the extended X-ray absorption fine structure (EXAFS)—is a technique that can be used to probe the short-range electronic and local structure around a specific atom of interest. While XANES provides useful information on the oxidation state and site symmetry of an element, EXAFS is able to give a significant amount of quantitative structural information, including the coordination number, the interatomic distance, and the Debye−Waller factor. Accordingly, XAS has been employed to probe the structure, symmetry, and coordination properties of various ILs.[42−45] Unlike XPS analyses, which must be done in an ultrahigh vacuum, XAS can be performed under a normal atmosphere. This facilitates an in situ XAS study, where the sample electrode is under certain applied potentials in the electrolyte and thus is closer to the real operation case.

Benedetti et al.[46] have studied the Li^+ intercalation in MnO_2 (for Li-ion battery application), using an electrochemical quartz crystal microbalance (EQCM), in 1-butyl-2,3-dimethyl-imidazolium−bis(trifluoromethanesulfonyl) imide (BMMI−TFSI) IL with addition of a lithium salt. Interestingly, they found that $BMMI^+$ and $TFSI^-$ could also participate in the charge compensation process in the interfacial region. How the $BMMI^+$ and $TFSI^-$ reacted with MnO_2, however, was not clarified. According to the mass change data (from EQCM), surface chemisorption and bulk insertion phenomena of the ions could hardly be distinguished. This investigation, for the first time, studies the pseudocapacitive mechanism of Mn oxide in butylmethylpyrrolidinium−dicyanamide (BMP−DCA) IL using both XPS and in situ XAS. The electronic and structural aspects of Mn oxide as a function of the applied potential are reported. Reversible insertion and desertion of DCA^- anions, which have never been explored, were confirmed upon the oxidation and reduction of the Mn oxide electrode in a potential range of 3 V. Within a reaction depth of approximately 50 nm, the quasi-linear DCA^- anions can be incorporated into the tunnels between the MnO_6 octahedral units and electroneutralize the Mn^{3+}/Mn^{4+} redox transition. On the other hand, the BMP^+ cations were just adsorbed on the electrode surface and did not penetrate into the oxide. The results of our study could help open up a new route for developing novel energy storage systems using IL electrolytes.

(23) Conway, B. E. Electrochemical Supercapacitors; Kluwer-Plenum: New York, 1999.
(24) Toupin, M.; Brousse, T.; Bélanger, D. *Chem. Mater.* **2004**, *16*, 3184.
(25) Chang, J. K.; Lee, M. T.; Tsai, W. T. *J. Power Sources* **2007**, *166*, 590.
(26) Nam, K. W.; Kim, M. G.; Kim, K. B. *J. Phys. Chem. C* **2007**, *111*, 749.
(27) Lee, H. Y.; Goodenough, J. B. *J. Solid State Chem.* **1999**, *144*, 220.
(28) Pang, S. C.; Anderson, M. A.; Chapman, T. W. *J. Electrochem. Soc.* **2000**, *147*, 444.
(29) Toupin, M.; Brousse, T.; Bélanger, D. *Chem. Mater.* **2002**, *14*, 3946.
(30) Hu, C. C.; Tsou, T. W. *Electrochem. Commun.* **2002**, *4*, 105.
(31) Rochefort, D.; Pont, A. L. *Electrochem. Commun.* **2006**, *8*, 1539.
(32) Fortunato, R.; Afonso, C. A. M.; Benavente, J.; Rodriguez-Castellon, E.; Crespo, J. G. J. *J. Membr. Sci.* **2005**, *256*, 216.
(33) Caporali, S.; Bardi, U.; Lavacchi, A. *J. Electron Spectrosc. Relat. Phenom.* **2005**, *151*, 4.
(34) Seyama, M.; Iwasaki, Y.; Tate, A.; Sugimoto, I. *Chem. Mater.* **2006**, *18*, 2656.
(35) Santos, C. S.; Baldelli, S. *J. Phys. Chem. B* **2007**, *111*, 4715.
(36) Smith, E. F.; Villar-Garcia, I. J.; Briggs, D.; Licence, P. *Chem Commun.* **2005**, 5633.
(37) Maier, F.; Gottfried, J. M.; Rossa, J.; Gerhard, D.; Schulz, P. S.; Schweiger, W.; Wasserscheid, P.; Steinrück, H.-P. *Angew. Chem., Int. Ed.* **2006**, *45*, 7778.
(38) Gottfried, J. M.; Maier, F.; Rossa, J.; Gerhard, D.; Schulz, P. S.; Wasserscheid, P.; Steinrück, H.-P. *Z. Phys. Chem.* **2006**, *220*, 1439.
(39) Silvester, D. S.; Broder, T. L.; Aldous, L.; Hardacre, C.; Crossley, A.; Compton, R. G. *Analyst* **2007**, *132*, 196.
(40) Kolbeck, C.; Killian, M.; Marier, F.; Paape, N.; Wasserscheid, P.; Steinrück, H.-P. *Langmuir* **2008**, *24*, 9500.
(41) Lockett, V.; Sedev, R.; Bassell, C.; Ralston, J. *Phys. Chem. Chem. Phys.* **2008**, *10*, 1330.
(42) Jensen, M. P.; Neuefeind, J.; Beitz, J. V.; Skanthakumar, S.; Soderholm, L. *J. Am. Chem. Soc.* **2003**, *125*, 15466.
(43) Hardacre, C. *Annu. Rev. Mater. Res.* **2005**, *35*, 29.
(44) Gaillard, G.; Chaumont, A.; Billard, I.; Hennig, C.; Ouadi, A.; Wipff, G. *Inorg. Chem.* **2007**, *46*, 4815.
(45) Bossé, E.; Auwer, C. D.; Berthon, C.; Guilbaud, P.; Grigoriev, M. S.; Nikitenko, S.; Naour, C. L.; Cannes, C.; Moisy, P. *Inorg. Chem.* **2008**, *47*, 5746.
(46) Benedetti, T. M.; Bazito, F. F. C.; Ponzio, E. A.; Torresi, R. M. *Langmuir* **2008**, *24*, 3602.

2. Experimental Section

Aprotic BMP−DCA IL, which is also used for electrodeposition applications,[47] was prepared and purified following a previously published method.[48] The IL was washed with acetone and dichloromethane, filtrated to remove NaCl precipitates, and then vacuum-dried at 393 K. The water content of the IL, measured with a Karl Fisher titrator, was approximately 100 ppm.

Mn oxide was anodically deposited[49,50] from 0.25 M Mn $(CH_3COO)_2$ aqueous plating solution at room temperature. A three-electrode electrochemical system was employed. A 1 cm × 1 cm Ni coupon (with a thickness of 120 μm and an exposed area of 1 cm^2) was etched in 2 M HCl solution at 80 °C, washed with pure water in an ultrasonic bath, and then used as the working electrode after drying. In addition, a platinum sheet and a saturated calomel electrode (SCE) were assembled as the counter electrode and reference electrode, respectively. The electrodeposition was performed under a constant potential of 0.8 V (vs SCE) to give a total passed charge of 0.4 Coulombs/cm^2. The typical mass of the deposited oxide, measured using a microbalance with an accuracy of 0.01 mg, was approximately 0.3 mg/cm^2 (with a thickness of about 1 μm). The surface morphology of the oxide electrode was examined with a scanning electron microscope (SEM, Hitachi SU-1500). An ultramicrotome was used to prepare a thin Mn oxide section (40−60 nm) for the transmission electron microscope (TEM, JEOL 3010) analyses. A camera length of 120 cm was adopted for the electron diffraction experiment.

The electrochemical properties of the Mn oxide electrode in BMP−DCA IL were characterized by cyclic voltammetry (CV) and chronopotentiometry (CP) at 25 °C in a nitrogen-purified glovebox (Vacuum Atmospheres Co.), where both the moisture and the oxygen content were maintained below 1 ppm. The reference electrode was a Pt wire placed in a fritted glass tube containing butylmethylpyrrolidinium−bis(trifluoromethylsulfony)imide IL that had a ferrocene/ferrocenium couple as a potential standard (Fc/Fc^+ = 50/50 mol %, showing a potential of + 0.55 V vs SHE). The counter electrode was a spiral Pt wire, which was directly immersed in the bulk BMP−DCA IL. The applied potential and current were regulated using an AUTOLAB potentiostat.

An X-ray photoelectron spectrometer (PHI 5000 VersaProbe) was used to probe the chemical state of BMP−DCA IL and the Mn oxide electrodes. Prior to the XPS analyses, the oxide electrodes underwent 10 CV scanning cycles and then were held at certain potentials of interest for 1 h. Afterward, the samples were cleaned with methanol, dried in an inert nitrogen gas atmosphere, and finally delivered to the XPS prelocked chamber using a transfer vessel, which was filled with high-purity nitrogen to prevent the samples from being exposed to air. Monochromatic Al Kα radiation (1486.6 eV) was used as the X-ray source. The pressure in the main chamber was below 1×10^{-9} Torr during the analyses.

The Mn oxide electrode was also investigated at various applied potentials in BMP−DCA IL with in situ XAS under the fluorescence mode. A sealed spectro-electrochemical cell with a fluorescence-transparent Kapton tape window was used. Before taking the spectra at a given potential, the electrode was kept at the set potential for 15 min to allow the oxide to reach a steady state. The XAS experiments were performed on beamline 17 C at the National Synchrotron Radiation Research Center (NSRRC) in Hsinchu, Taiwan. The storage ring was operated with an electron energy of 1.5 GeV and a current between 100 and 200 mA. A Si(111) double-crystal monochromator was employed for energy selection. The X-ray absorption energy was calibrated using the first inflection point of the Mn K-edge main absorption region of a metallic Mn foil (6539.0 eV), which was measured before every XAS scan.

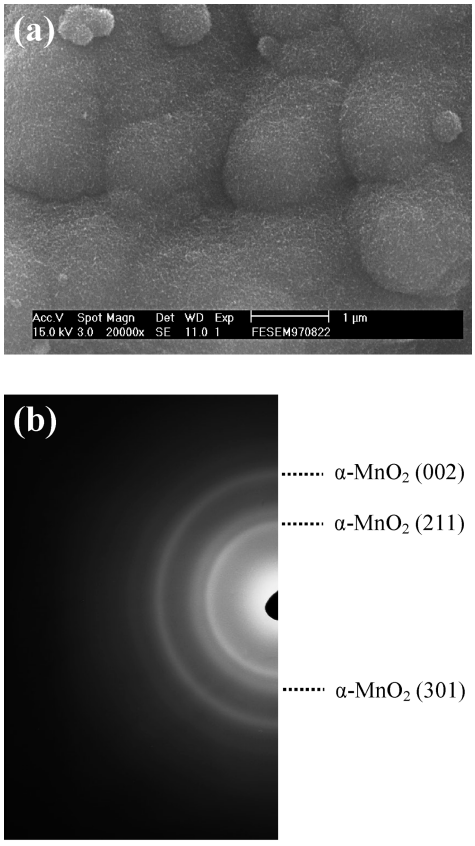

Figure 1. (a) SEM micrograph of the anodically deposited Mn oxide electrode. (b) The electron diffraction pattern of the Mn oxide examined with a TEM.

3. Results and Discussion

Figure 1a shows the SEM micrograph of the anodically deposited Mn oxide. A granular morphology can be clearly seen. The crack could be attributed to the shrinkage of the deposited oxide during drying and/or vacuuming. A close examination of this photo reveals that the deposit is actually composed of interweaving oxide nanowhiskers. Similar microstructure has also been observed in the literature.[51,52] Figure 1b shows the electron diffraction data taken from the prepared Mn oxide. The three signals in the pattern are associated with the (211), (301), and (002) diffraction

(47) Deng, M. J.; Chen, P. Y.; Leong, T. I.; Sun, I. W.; Chang, J. K.; Tsai, W. T. *Electrochem. Commun.* **2008**, *10*, 213.
(48) MacFarlane, D. R.; Forsyth, S. A.; Golding, J.; Deacon, G. B. *Green Chem.* **2002**, *4*, 444.
(49) Chang, J. K.; Tsai, W. T. *J. Electrochem. Soc.* **2003**, *150*, A1333.
(50) Chang, J. K.; Chen, Y. L.; Tsai, W. T. *J. Power Sources* **2004**, *135*, 344.
(51) Hu, C. C.; Wang, C. C. *J. Electrochem. Soc.* **2003**, *150*, A1079.
(52) Prasad, K. R.; Miura, N. *J. Power Sources* **2004**, *135*, 354.

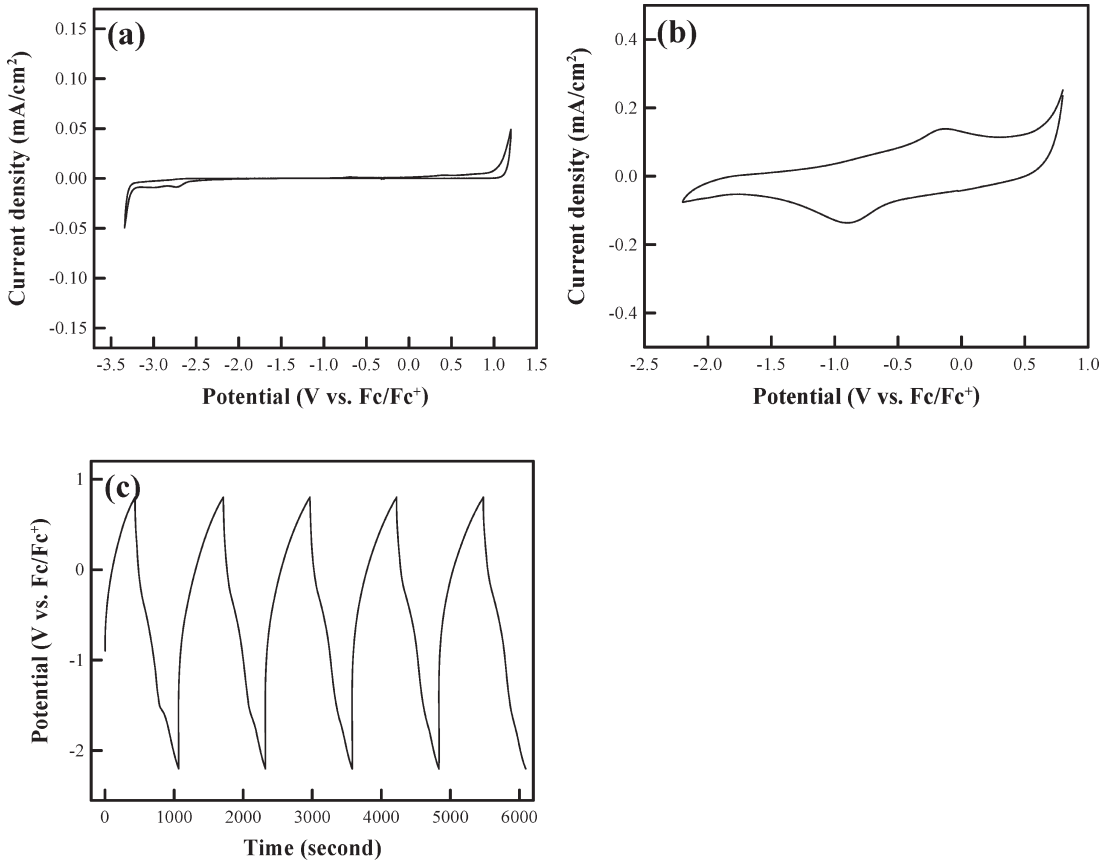

Figure 2. Cyclic voltammograms of (a) an inert glassy carbon electrode and (b) the Mn oxide electrode recorded in BMP−DCA IL at a potential sweep rate of 5 mV/s. (c) Chronopotentiogram for five charge−discharge cycles of the Mn oxide electrode measured at an applied current density of ± 0.1 mA/cm^2.

planes of α-MnO_2 (JCPDS 44-0141), respectively, as marked in the figure. However, the dim rings indicate the nanocrystalline and nonstoichiometric nature of the prepared Mn oxide.

Figure 2a shows the cyclic voltammogram of BMP−DCA IL recorded on an inert glassy carbon electrode at a potential sweep rate of 5 mV/s. A very wide electrochemical stability window, extending from approximately −3.3 V to +1.2 V, was found for the IL. Within the breakdown limits, the tiny current on the double-layer charging background could be associated with the electrolysis (or decomposition) of some electroactive impurity in the IL. The much wider potential window compared to that of a conventional aqueous solution (i.e., typically ∼1 V) makes the IL a promising electrolyte for high cell-voltage energy storage devices. Figure 2b shows the cyclic voltammogram of the Mn oxide electrode measured in BMP−DCA IL. The cathodic and anodic irreversible reactions, probably associated with oxide dissolution, were found beyond −2.2 V and +0.8 V, respectively. However, in an operative region of approximately 3 V, a symmetric CV curve, characterized by a very broad anodic and cathodic pair (with similar integrated charges), was noted. The quasi-rectangular response of the CV shape, which represents pseudocapacitive behavior, could thus be attributed to a continuous and reversible faradic redox transition of Mn oxide over the potential range in BMP−DCA IL. Electrochemical properties of the oxide electrode in the IL were also evaluated by CP; both the charging (anodic) and discharging (cathodic) current densities were set at 0.1 mA/cm^2. The obtained chronopotentiogram for five charge−discharge cycles in a potential range of −2.2 V to +0.8 is shown in Figure 2c. As can be seen, the charge and discharge branches are essentially linear and symmetric, again revealing a pseudocapacitive performance of the oxide electrode. The specific capacitance of the oxide can be calculated according to the following equation:

$$C = I/(\Delta E/\Delta t)w \quad (1)$$

where I is the applied current (0.1 mA), ΔE is the potential sweep range (3 V), Δt is the discharge time, and w is the mass of the oxide. The measured specific capacitance of Mn oxide in BMP−DCA IL was 70 F/g. It should be noted that although this value is only about one-third of that typically found in aqueous electrolytes,[27,30,49] the high electrode operative potential (∼3 V) in the IL allows for a higher energy density and a higher power density of a capacitor since both the parameters depend on the square of the cell voltage. To evaluate the charge−discharge stability of Mn oxide in BMP−DCA IL, 500 redox CP cycles were performed. It was found that the retained capacitance was as high as 95% as compared to the initial value (from first cycle). In contrast, our previous studies indicated that, in aqueous KCl and Na_2SO_4 electrolyte, only approximately 75% of the initial capacitance can be maintained after

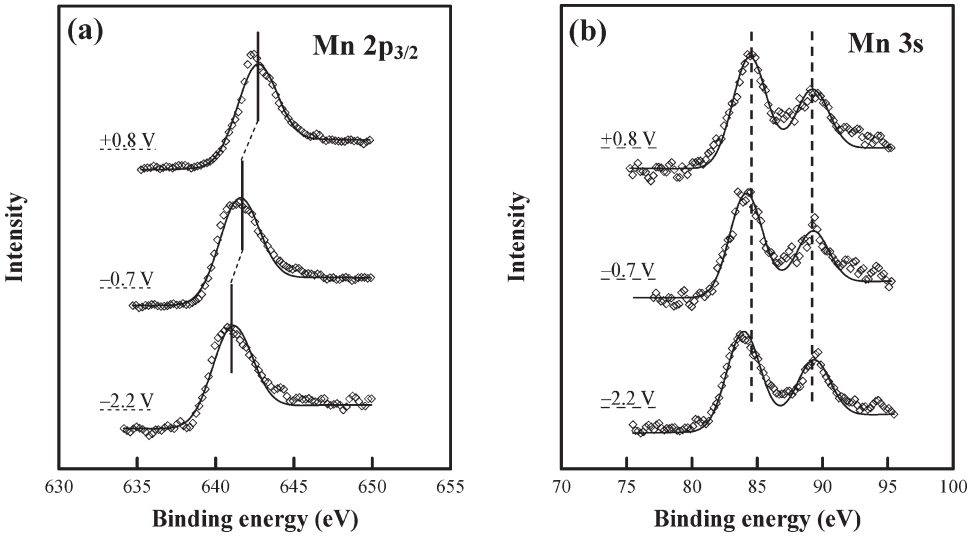

Figure 3. (a) Mn $2p_{3/2}$ and (b) Mn 3s XPS spectra of the Mn oxide electrodes previously polarized at +0.8 V, −0.7, and −2.2 V in BMP−DCA IL.

500 redox cycles.[53] The fading can be mainly attributed to the partial dissolution of Mn oxide in the aqueous solution.[54] The superior electrochemical reversibility and durability of Mn oxide in BMP−DCA IL may be associated with the chemical benignity of the IL and with the extremely low solubility of Mn oxide in the IL. The obtained experimental results suggest that BMP−DCA IL is a potential electrolyte for long-life charge storage devices based on Mn oxide electrodes.

XPS was used to examine the valent state of Mn oxide under various applied potentials in the IL. Figure 3a shows the Mn $2p_{3/2}$ spectra of the oxides previously polarized at +0.8 V, −0.7 V, and −2.2 V, respectively; a chemical shift can be clearly recognized. Specifically, a higher applied potential led to a higher binding energy of the Mn $2p_{3/2}$ electron, suggesting that the Mn oxide was in a higher oxidation state.[55] It is known that the valence of Mn can be more precisely identified by measuring the multiplet splitting width of two Mn 3s XPS peaks.[15] Therefore, the spectra of this orbital were also acquired for the three oxide electrodes; the obtained data are shown in Figure 3b. According to the analytical data, the ΔE values for the +0.8 V, −0.7 V, and −2.2 V polarized electrodes are 4.82 eV, 5.12 eV, and 5.38 eV, respectively. The exchange interaction between the core level electron (3s) and the unpaired electrons in the valence band (3d) results in the peak separation (ΔE) of the Mn 3s spectrum upon photoelectron ejection.[56,57] A lower valence of Mn leads to a wider splitting of the Mn 3s peaks. As reported by Chigane et al.,[15] Mn_2O_3 has a ΔE of 5.41 eV while MnO_2 has a ΔE of 4.78 eV. The comparison results indicate that when the applied potential was varied from −2.2 V to +0.8 V, the oxidation state of Mn oxide gradually increased from trivalence to tetravalence. This confirms that the broad redox pair observed in Figure 2b is associated with a Mn^{3+}/Mn^{4+} faradic transition. Rochefort et al.[31] has suggested that RuO_2 cannot perform any redox transition in aprotic 1-ethyl-3-methylimidazolium tetrafluoroborate (EMI−BF_4) IL. Apparently, the chemistry of the IL electrolyte and the tunnel structure of Mn oxide play important roles in governing the electrochemical properties; both of these issues are examined in the following sections.

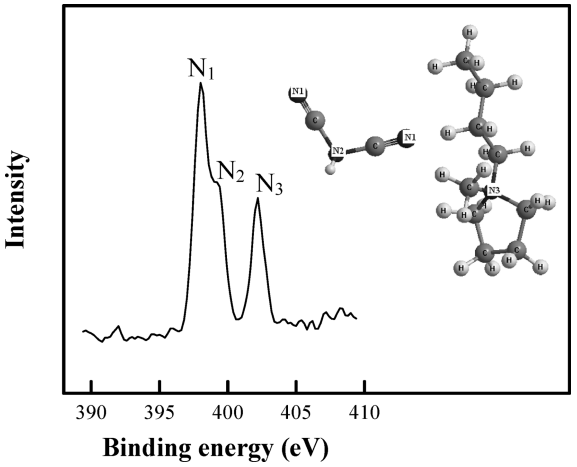

Figure 4. XPS N 1s spectrum of BMP−DCA IL. The inset shows the chemical structure of the IL.

Since neither proton nor alkali cations (Li^+, Na^+, or K^+) exist in BMP−DCA IL, the pseudocapacitive mechanism of Mn oxide must be different from that observed in aqueous electrolytes. To understand what kinds of ions compensate the Mn oxidation state variation during the redox process, the chemical characteristics of BMP−DCA IL were preliminarily analyzed with XPS. The extremely low vapor pressure of the IL makes it stable in the ultrahigh vacuum XPS analytical chamber. Figure 4 shows the obtained N 1s spectrum of BMP−DCA IL. As a result of the different chemical environments of N in the IL, as shown in the inset, three N peaks with distinct binding energies can be recognized. While NC (N_1) and NC_2 (N_2)

(53) Chang, J. K.; Lin, C. T.; Tsai, W. T. *Electrochem. Commun.* **2004**, *6*, 666.
(54) Chang, J. K.; Lee, M. T.; Huang, C. H.; Tsai, W. T. *Mater. Chem. Phys.* **2008**, *108*, 124.
(55) Hasemi, T.; Brinkman, A. W. *J. Mater. Res.* **1992**, *7*, 1278.
(56) Carver, J. C.; Schweitzer, G. K.; Carlson, T. A. *J. Chem. Phys.* **1972**, *57*, 973.
(57) Oku, M.; Hirokawa, K.; Ikeda, S. *J. Electron Spectrosc. Relat. Phenom.* **1975**, *7*, 465.

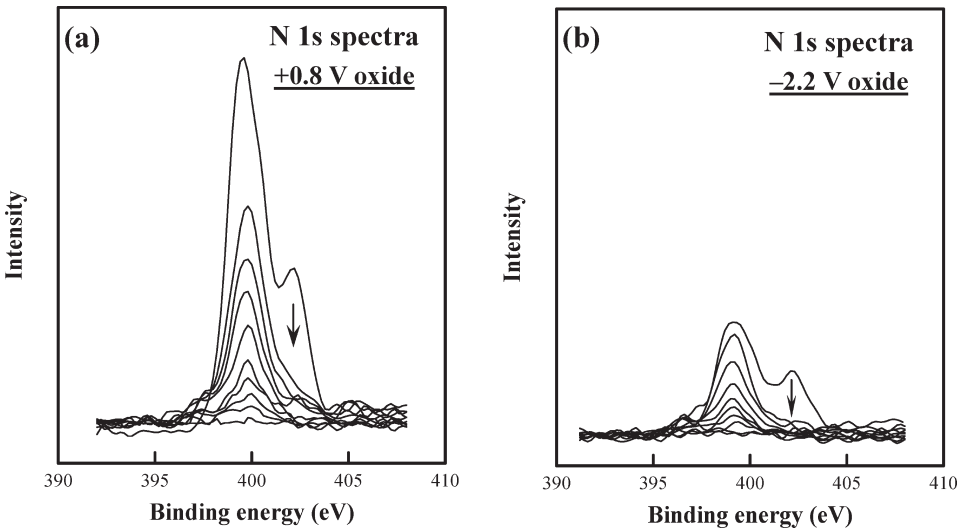

Figure 5. XPS N 1s depth-profiling spectra taken from the Mn oxide electrodes previously polarized at (a) +0.8 V and (b) −2.2 V in BMP−DCA IL.

bonds in the DCA^- anion have binding energies at 398.0 and 399.3 eV, respectively, the NC_3 (N_3) bond in the BMP^+ cation has a binding energy at 402.2 eV. It is also noted that the relative area under of the three peaks is approximately 2:1:1, which is consistent with the stoichiometric ratio of N_1, N_2, and N_3 in BMP−DCA IL.

Figure 5a shows the depth-profiling N 1s spectra taken from the +0.8 V-polarized oxide electrode. As compared to Figure 4, it can be recognized that, on the topmost layer, the binding energy of the N_1 peak clearly changes to 399.5 eV while the N_3 peak remains unchanged at 402.2 eV. It was also found that the positive shift of N_1 was more pronounced than that of N_2; consequently, the two peaks almost merge into one. The analytical results suggest that the DCA^- anion bonded with Mn, preferredly via the N_1 site, and experienced a chemical state variation. On the other hand, the BMP^+ cation did not seem to have significant interaction with the Mn oxide electode. The depth profiling analysis was performed using Ar^+ sputtering. The removal rate per sputtering shot (3 s) was measured to be approximately 5 nm for SiO_2 film. Nine serial profiles of N 1s spectra are also shown in Figure 5a. The signal from BMP^+ was found to disappear after only one shot of Ar^+ sputtering, indicating that the cation was just adsorbed on the electrode surface. In contrast, the DCA^- anion penetrated into Mn oxide. Although the DCA^- intensity decreased with depth, the incorporated thickness was about 50 nm, assuming that the sputtering rate of Mn oxide is similar to that of SiO_2. Figure 5b shows the spectra obtained from the −2.2 V-polarized oxide; as can be seen, the surface is relatively enriched with BMP^+, as compared to that of the +0.8-polarized sample, due to charge attraction. However, it was confirmed that the BMP^+ signal, also located at 402.2 eV, was easily removed upon Ar^+ sputtering, revealing that the cation cannot really enter the oxide. In addition, the intensity from DCA^- was much lower than that found in Figure 5a because this anion was extracted from the oxide under the cathodic applied potential. The experimental results indicate that the bended (or quasi-linear) DCA^- anion, instead of the huge BMP^+ cation with an imidazolium ring, is the working species that can incorporate into Mn oxide, compensate the Mn valent state variation, and thus contribute to the pseudocapacitance.

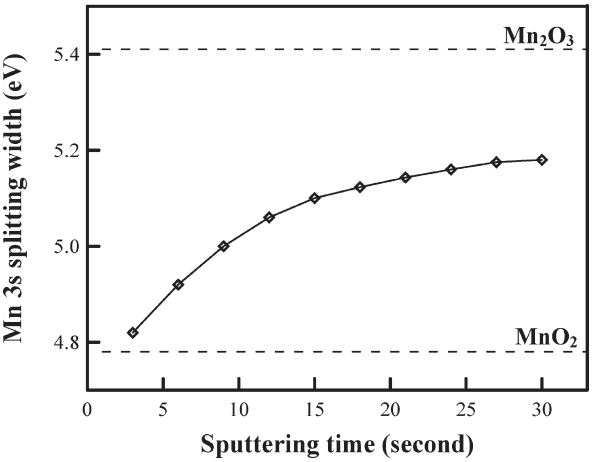

Figure 6. Mn 3s XPS splitting width of the +0.8 V-polarized oxide electrode as a function of Ar^+ sputtering time.

Figure 6 summarizes the splitting width of the Mn 3s XPS spectra and the corresponding Mn valent state for the +0.8 V-polarized electrode as a function of the Ar^+ sputtering time. As shown, ΔE initially increases with depth and then reaches a steady value. The analytical results indicate that while the outer-surface Mn was anodized to tetravalence, the underlying oxide was a mixture of trivalence and tetravalence. The data in Figure 6 reveal that the reaction layer of Mn oxide in BMP−DCA IL is approximately 50 nm thick, which is consistent with the N incorporated depth. It was confirmed that the incorporation of DCA^- anions was charge balanced by an oxidation process of Mn^{3+} (to Mn^{4+}) in the oxide electrode.

The charge storage mechanism of Mn oxide was further examined using in situ XAS, which allows the chemical state variation under certain potentials of interest to be directly examined in IL. Figure 7 shows the configuration of the spectroelectrochemical cell used in this investigation.

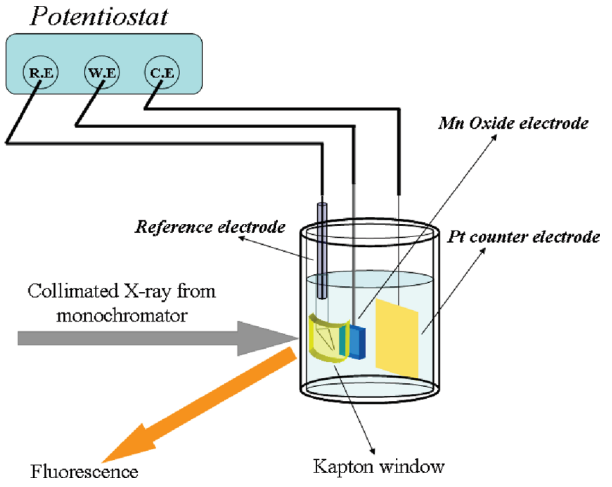

Figure 7. Configuration of the spectroelectrochemical cell used in the in situ XAS studies.

In the cylinder, which has a diameter of 2 cm, the oxide electrode was placed facing the X-ray window. The distances between the sample and the reference and counter electrodes were approximately 0.5 cm. Figure 8a shows three serial Mn K-edge XANES spectra of the Mn oxide electrode measured in the sequence: −2.2 V, +0.8 V, and then back to −2.2 V. As demonstrated, each spectrum can be divided into a pre-edge region (A), a main edge region (B), and a peak region (C), followed by an EXAFS oscillation. The pre-edge adsorption peak is assigned to the electronic excitation from a 1s core state to an unoccupied 3d orbital. Since the 1s → 3d jump is a formally electric dipole-forbidden transition in an ideal octahedral symmetry, the intensity is weak. The main edge and the absorption peak are respectively ascribed to the electric dipole-allowed transition of a 1s core electron to an unoccupied 4p bound state with and without a shakedown process, which originated from ligand-to-metal charge transfer. Accordingly, the final states of Mn^{4+} are $1s^1c3d^4L4p^1$ and $1s^1c3d^34p^1$, respectively, where c is a 1s core hole and L is an oxygen 2p ligand hole. As shown in Figure 8a, the three spectra do not exhibit considerable difference in shape, revealing a similarity in the structural characteristics of Mn under various applied potentials. However, an energy shift of the adsorption edge, which was toward higher energy with increasing applied potential and almost returned to its initial position as the potential was decreased, can be clearly seen in this figure. According to the literature,[58,59] the valent state of Mn can be identified by the absorption threshold energy (E_0), which can be obtained from the first inflection point on the main absorption edge. This so-called chemical shift is related to the increase in binding energy of the core-level electron with increasing oxidation state, which is in turn caused by the reduced screening of the core level by valence electrons.[58] The E_0 values of the three serial spectra in Figure 8a are found to be 6549.8 eV, 6551.5 eV, and 6549.9 eV, respectively. Reference samples such as MnO(II), Mn_2O_3(III), and MnO_2(IV) were also analyzed;

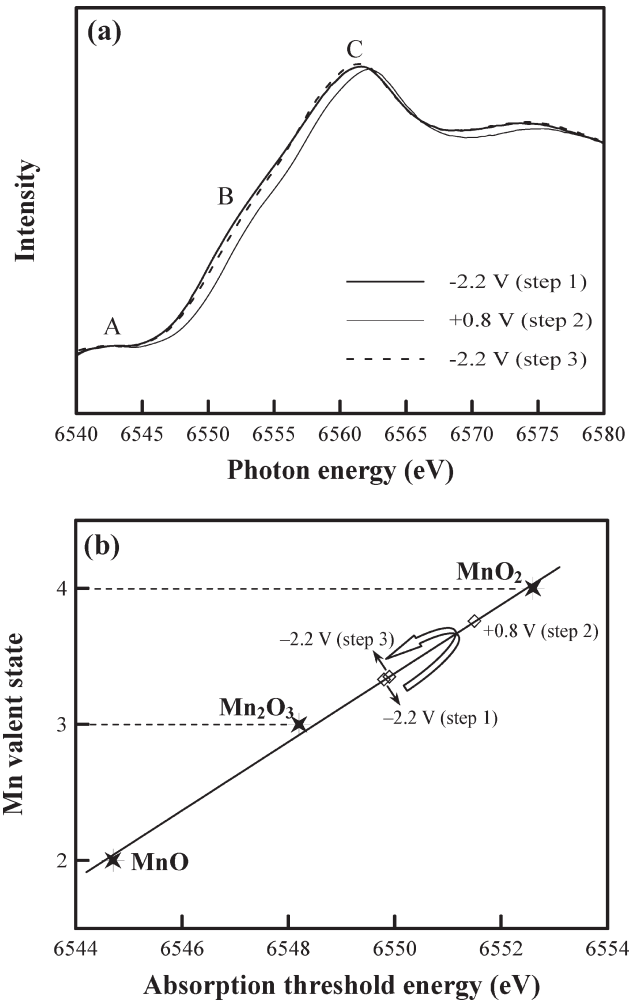

Figure 8. (a) In situ Mn K-edge XANES spectra of the oxide electrode measured at the applied potentials in sequence of −2.2 V, +0.8 V, and then back to −2.2 V. (b) The variation of the Mn valent state with respect with the applied potential. Three reference samples with their E_0 values are also shown.

their E_0 values were at 6544.7 eV, 6548.2 eV, and 6552.6 eV, respectively. These analytical data are compared in Figure 8b. Since an ideal linear relationship ($R^2 > 0.99$) between E_0 and the Mn oxidation state was found, as proposed in the literature,[60] the average valence of Mn can be quantitatively determined. The calculated results indicate that the Mn oxide was initially at a valent state of +3.33 (at −2.2 V), then oxidized to +3.76 (at +0.8 V), and finally reduced again to +3.35 valence (at −2.2 V). Accordingly, a reversibility of the electrochemical reaction of Mn oxide over a 3 V potential range in BMP−DCA IL was confirmed. This feature could also explain the great redox stability of the oxide electrode during the charging−discharging cycling. It is noteworthy that the Mn valence variation between the −2.2 V and +0.8 V electrodes was approximately 0.42, which is much less than that (~1) found in the XPS analyses. This deviation can be explained by considering the difference of probing depths between the two techniques. Since the fluorescence mode was used in the XAS study, the analytical signal was generally collected

(58) Belli, M.; Scafati, A.; Bianconi, A.; Mobilio, S.; Palladino, L.; Reale, A.; Burattini, E. *Solid State Commun.* **1980**, *35*, 355.
(59) Ghigna, P.; Flor, G.; Spinolo, G. *J. Solid State Chem.* **2000**, *149*, 252.
(60) Farges, F. *Phys. Rev. B* **2005**, *71*, 155109.

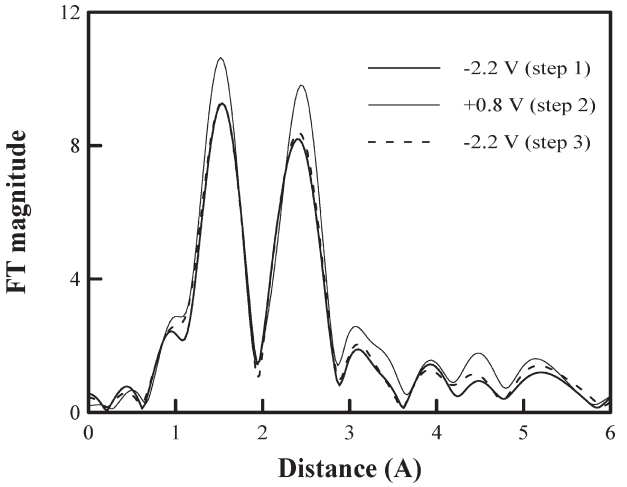

Figure 9. In situ Mn K-edge EXAFS spectra of the oxide electrode measured at the applied potentials in sequence of −2.2 V, +0.8 V, and then back to −2.2 V.

from a submicrometer depth beneath the oxide surface,[61] which is deeper than that (typically <10 nm) of XPS. Because the reaction layer was only about 50 nm, as indicated by the XPS depth profiling analyses, the valent state evaluated using XAS is an average value and may involve the underlying unreacted Mn oxide.

Figure 9 shows the Fourier transformed (FT) magnitudes of Mn K-edge EXAFS spectra of the oxide electrode measured at applied potentials in the sequence: −2.2 V → +0.8 V → −2.2 V. The EXAFS spectrum is the amplitude summation of the constructive and destructive scattering, which are influenced by the local environment and the occupied atoms surrounding the target absorber. The first peak of the spectra around 1.5 Å (without phase shift correction) is due to an interaction with oxygen in the first coordination shell. The second peak located near 2.5 Å corresponds to the nearest neighboring Mn atoms in the second coordination shell (i.e., in the next octahedral unit). The data in Figure 9 indicate the following four features. (1) A higher applied potential led to an increase in the magnitude of the Mn−O peak. This increase was ascribed to a local structure change induced by the Mn oxidation. Since Mn^{3+} is a Jahn−Teller distorted site,[62] oxidation of Mn^{3+} to non-Jahn−Teller Mn^{4+} led to relatively symmetric oxygen distribution. Moreover, the oxidation of Mn also increased the regularity of the MnO_6 octahedral framework. As a result, the magnitude of the FT Mn−O peak increased at the higher applied potential, that is, +0.8 V. (2) Increasing the potential to +0.8 V shifted the Mn−O peak toward a lower interatomic distance. The bond length decrease for Mn−O supports an oxidation transition. The ionic radius of Mn^{3+} (0.64 Å) is larger than that of Mn^{4+} (0.53 Å);[63] this explains the shrinkage of the first coordination shell. (3) Oxidation of the electrode to +0.8 V led to a clear increase of the Mn−Mn bond length. This expansion of the second coordination shell, associated with a distance increase between the next MnO_6 octahedral unit, can be attributed to the insertion of DCA^- anions into the oxide structure. However, due to the very weak backscattering amplitude of the photoelectrons from carbon and nitrogen light atoms (in DCA^-), their signals were neglected in the EXAFS spectra. In a Li^+ operative electrolyte, it has been observed that the two M−O and M−M peaks (M denotes metal) shift in the same direction; that is, toward longer M−O and M−M interatomic distances upon lithiation and back to shorter distances upon delithiation.[64,65] The opposite shift directions of the Mn−O and Mn−Mn peaks in Figure 9 indicate that anions are the primary working species that insert/desert into/from the Mn oxide structure and cause the electrochemical redox reaction. (4) Reducing the electrode back to −2.2 V resulted in the EXAFS spectrum returning to its original state. The reversible change in the FT peak position and intensity reveals the reversibility of the local electronic and geometric structures around the central Mn atom during the charge and discharge. Accordingly, a reversible anion insertion and desertion electrochemical reaction can be proposed as follows:

$$MnO_{2-x}(DCA)_{2x} + 2xe^- \leftrightarrow MnO_{2-x} + 2xDCA^- \quad (x \le 0.5) \quad (2)$$

This faradic redox reaction causes the pseudocapacitive behavior of the Mn oxide electrode in BMP−DCA IL electrolyte.

4. Conclusion

Pseudocapacitive performance of Mn oxide was confirmed in aprotic BMP−DCA IL. Within a potential range of 3 V, a specific capacitance of 70 F/g and great cyclic stability of the oxide were obtained. XPS and in situ XAS were used to examine the charge storage mechanism in the IL. The analytical results indicate that the Mn^{3+}/Mn^{4+} redox transition during the charge−discharge process was charge compensated by the reversible insertion/desertion reaction of DCA^- anions into/from the tunnels between the MnO_6 octahedral units. The BMP^+ cations were just adsorbed on the electrode surface and did not penetrate into the oxide. This paper not only provides an effective approach to understand the electrochemical mechanism involving an IL electrolyte but also opens up a new route for developing novel energy storage systems.

Acknowledgment. The authors would like to thank the National Science Council of the Republic of China for financially supporting this research (under Contract No. NSC 98-ET-E-006-009-ET).

(61) Garg, H. B.; Stern, E. A.; Norman, D. X-ray Absorption in Bulk and Surfaces; World Scientific Publishing Co.: Singapore, 1994.
(62) Shiraishi, Y.; Nakai, I.; Tsubata, T.; Himeda, T.; Nishikawa, F. *J. Solid State Chem.* **1997**, *133*, 587.
(63) Shannon, R. D. *Acta Crystallogr.* **1976**, *32*, 751.
(64) Yoon, W.-S.; Grey, C. P.; Balasubramanian, M.; Yang, X.-Q.; McBreen, J. *Chem. Mater.* **2003**, *15*, 3161.
(65) Tsai, Y. W.; Hwang, B. J.; Ceder, G.; Sheu, H. S.; Liu, D. G.; Lee, J. F. *Chem. Mater.* **2005**, *17*, 3191.